

## Accepted Manuscript

Transition metal complexes of 2-(2-(1H-benzo[d]imidazol-2-yl)hydrazono)propan-1-ol: Synthesis, Characterization, Crystal structures and anti-tuberculosis assay with docking studies

Vinayak Kamat, Dhoolesh Kokare, Krishna Naik, Avinash Kotian, S. Naveen, Sheshagiri R. Dixit, N.K. Lokanath, Shrinivas D Joshi, Vidyanand K. Revankar

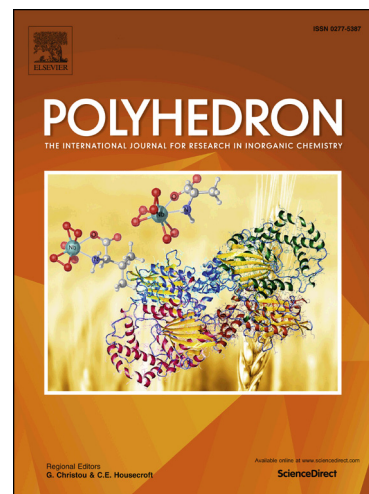
PII: S0277-5387(17)30120-1  
DOI: <http://dx.doi.org/10.1016/j.poly.2017.02.010>  
Reference: POLY 12477

To appear in: *Polyhedron*

Received Date: 19 December 2016  
Revised Date: 8 February 2017  
Accepted Date: 9 February 2017

Please cite this article as: V. Kamat, D. Kokare, K. Naik, A. Kotian, S. Naveen, S.R. Dixit, N.K. Lokanath, S.D. Joshi, V.K. Revankar, Transition metal complexes of 2-(2-(1H-benzo[d]imidazol-2-yl)hydrazono)propan-1-ol: Synthesis, Characterization, Crystal structures and anti-tuberculosis assay with docking studies, *Polyhedron* (2017), doi: <http://dx.doi.org/10.1016/j.poly.2017.02.010>

This is a PDF file of an unedited manuscript that has been accepted for publication. As a service to our customers we are providing this early version of the manuscript. The manuscript will undergo copyediting, typesetting, and review of the resulting proof before it is published in its final form. Please note that during the production process errors may be discovered which could affect the content, and all legal disclaimers that apply to the journal pertain.



**Transition metal complexes of 2-(2-(1H-benzo[d]imidazol-2-yl)hydrazono)propan-1-ol :  
Synthesis, Characterization, Crystal structures and anti-tuberculosis assay with docking studies**

Vinayak Kamat<sup>a</sup>, Dhoolesh Kokare<sup>a</sup>, Krishna Naik<sup>a</sup>, Avinash Kotian<sup>a</sup>, Naveen S.<sup>b</sup>, Sheshagiri R.  
Dixit<sup>c</sup>, Lokanath N.K.<sup>d</sup>, Shrinivas D Joshi<sup>c</sup> and Vidyanand K. Revankar<sup>a\*</sup>

<sup>a</sup> Department of Chemistry, Karnatak University, Dharwad-580003, India.

<sup>b</sup> Institution of Excellence, Vijnana Bhavan, University of Mysore, Manasagangotri, Mysuru-570 006, India.

<sup>c</sup> Novel Drug Design and Discovery Laboratory, Department of Pharmaceutical Chemistry, S.E.T.'s College of Pharmacy, Sangolli Rayanna Nagar, Dharwad-580 002, Karnataka, India.

<sup>d</sup> Department of Studies in Physics, University of Mysore, Manasagangotri, Mysuru-570 006, India.

\* Corresponding author

**Abstract :** Transition metal coordination complexes of Co(II), Ni(II), Cu(II) and Zn(II) with a newly designed ligand, 2-(2-(1H-benzo[d]imidazol-2-yl)hydrazono)propan-1-ol have been synthesized and characterized using various spectro-analytical techniques. The molecular structures of Co(II), Cu(II) and Zn(II) complexes are determined by single-crystal X-ray diffraction method. The metal to ligand stoichiometry has been found to be 1:2 in the case of Cobalt(II), Nickel(II) and Zinc(II) whereas 1:1 in the case of Copper(II) complex. The newly synthesized ligand and complexes have been assessed for their growth inhibiting potencies against H37Rv strain of *Mycobacterium tuberculosis*. The copper and cobalt complexes have emerged to be potent in vitro growth inhibitors of H37Rv. All the complexes are inhibiting the growth of other tested common microbial flora to a significantly lesser extent, making them selective towards H37Rv in the preliminary analysis. The Consensus scores obtained by the docking studies of the molecules to the target protein enoyl acyl carrier protein reductase of *M. tuberculosis* H37Rv are in good agreement with the obtained MIC values.

**Key Words :** 2-(2-(1H-benzo[d]imidazol-2-yl)hydrazono)propan-1-ol, 2-hydrazinobenzimidazole, transition metal complexes, antituberculosis against H37Rv, enoyl acyl carrier protein reductase of *M. tuberculosis* H37Rv, docking of metal complexes.

**Highlights :**

- A novel benzimidazole based tridentate ligand 2-(2-(1H-benzo[d]imidazol-2-yl)hydrazono)propan-1-ol is synthesized and characterized.
- Co(II), Ni(II), Cu(II) and Zn(II) metal complexes of the ligand are synthesized and characterized by the single crystal X-ray diffraction method.
- Ligand and complexes are tested for their antibacterial (including antitubercular) and antifungal potencies.
- The observed in-vitro results are supported by docking studies on target protein enoyl acyl carrier protein reductase of *M. tuberculosis* H37Rv.

**1. Introduction**

Transition metal complexes of hydrazone based Schiff base ligands are of particular interest in the field of coordination chemistry. Hence these have been reported in the literature for a long time [1]. In recent years, Schiff bases with nitrogen and oxygen donors have drawn special attention due to their structural lability, ability to possess unusual configurations, and their sensitivity to molecular environments [2, 3].

Ever since the discovery of cisplatin, years have witnessed the progress in biological applications of transition metal coordination complexes [4]. Manipulation of the properties of biopotent ligands by complexation has continued to be an active field for clinical therapeutic applications [5]. Versatility in oxidation states, ease of complexation, a variety of electronic properties, ligand-induced tunability of geometry and coordination numbers makes transition metals suitable for this purpose over the main group elements [6]. Transition metal complexes of vanadium as antidiabetic agents [7-9], copper complexes as plausible anticancer agents [10], cobalt and copper complexes as antimicrobial/antitubercular agents are few of well-established examples [11, 12].

H37Rv is the most virulent and most studied strain of TB in research laboratories. Recently, substituted benzimidazole derivatives have emerged to be the promising class for the growth inhibition of H37Rv [13-15]. Moreover, these organic moieties have undergone excellent activity enhancement upon metallation [16, 17]. Literature even reveals significant successes of copper complexes as anti-TB agents, especially with potential tridentate chelators [18, 19]. Considering these facts, herein we report the synthesis, characterization and crystal structures of novel transition metal complexes of a designed tridentate N,N,O-chelator.

## 2. Experimental

### 2.1. General

Hydroxyacetone obtained from Sigma-Aldrich and other reagents obtained from Spectrochem were used as supplied. Solvents were purified and dried according to standard procedures. The metal salts used were in their hydrated form, i.e.,  $\text{CoCl}_2 \cdot 6\text{H}_2\text{O}$ ,  $\text{NiCl}_2 \cdot 6\text{H}_2\text{O}$ ,  $\text{CuCl}_2 \cdot 2\text{H}_2\text{O}$  and  $\text{Zn}(\text{NO}_3)_2 \cdot 6\text{H}_2\text{O}$ . The  $^1\text{H}$  and  $^{13}\text{C}$  NMR spectra were recorded on AGILENT VNMRS-400 spectrometer, in  $\text{DMSO}-d_6$  solvent. Infrared spectra of the ligand and its metal complexes were recorded in KBr discs in the region  $4000\text{--}400\text{ cm}^{-1}$  on a Nicolet-6700 FT-IR spectrometer. The CHN analysis was carried out using a Thermo quest elemental analyzer. The solution state UV-Vis spectra of all the compounds in DMF were recorded on a JASCO V-670 50 UV-Vis spectrophotometer. Thermal behavior of the metal complexes was analyzed on a Universal V2.4F TA instrument, from room temperature to a final temperature of  $1000\text{ }^\circ\text{C}$  at the heating rate of  $10\text{ }^\circ\text{C}/\text{min}$ . The cyclic voltammetric experiments were carried out with a three electrode apparatus using a CHI630D electrochemical analyzer (USA). The EI mass spectrum of the ligand was obtained with a Shimadzu GCMS-QP2010S spectrometer. The ESI mass spectral data for all the complexes were obtained using a Waters UPLCTQD mass spectrometer. The molar conductivity measurements of 1mM complex solutions in DMF were carried out on equiptronics EQ-665 conductivity bridge.

### 2.2. Single crystal X-ray crystallography

Single crystals of suitable dimensions were chosen carefully for X-ray diffraction studies. The X-ray intensity data were collected on a Bruker Proteum2 CCD diffractometer equipped with an X-ray generator operating at 45 kV and 10 mA, using  $\text{Cu-K}\alpha$  radiation of wavelength  $1.54178\text{ \AA}$  or on a Bruker APEX2 CCD area-detector diffractometer using graphite monochromated  $\text{Mo-K}\alpha$  radiation of wavelength  $0.71073\text{ \AA}$ . The Data were collected for 24 frames per set with different settings of  $\phi$  ( $0^\circ$  and  $90^\circ$ ), keeping the scan width of  $0.5^\circ$ , exposure time of 2 s, the sample to detector distance of 45.10 mm and  $2\theta$  value at  $46.6^\circ$ . The complete data sets were processed using SAINT PLUS [20]. The structures were solved by direct methods and refined by a full-matrix least squares method on F2 using SHELXS and SHELXL programs [21]. The geometrical calculations were carried out using the program PLATON [22]. The molecular and packing diagrams were generated using the software MERCURY-3.8 [23]. A summary of the crystallographic data is tabulated in table 1.

| Identification code | $[\text{CoL}_2]\text{Cl}_2$                                   | $[\text{CuLCl}_2]$  | $[\text{ZnL}_2](\text{NO}_3)_2$                              |
|---------------------|---|---|--|
| Empirical formula   | $\text{C}_{20}\text{H}_{27}\text{Cl}_2\text{CoN}_8\text{O}_2$ | $\text{C}_{10}\text{H}_{12}\text{Cl}_2\text{CuN}_4\text{O}$ | $\text{C}_{22}\text{H}_{30}\text{N}_{10}\text{O}_9\text{Zn}$ |
| Formula weight      | 538.30  | 338.68  | 643.93   |
| Wavelength          | $0.71073\text{ \AA}$  | $1.54178\text{ \AA}$  | $1.54178\text{ \AA}$   |

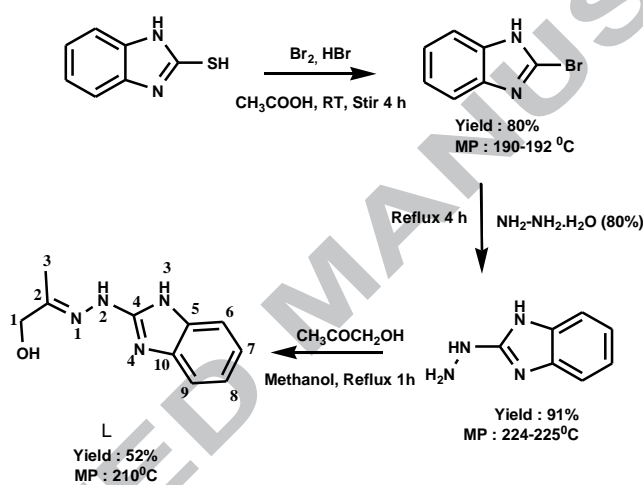
|                                   |   |   |   |
|-----------------------------------|---|---|---|
| Crystal system                    | Monoclinic                                  | Monoclinic                                  | Triclinic                                   |
| Space group                       | $P2_1/n$                                    | $C2/c$                                      | $P-1$                                       |
| Unit cell dimensions              |   |   |   |
| a                                 | 8.3006(3) Å                                 | 10.9099(3) Å                                | 8.1759(6) Å                                 |
| b                                 | 9.5927(4) Å                                 | 11.4342(3) Å                                | 9.1983(6) Å                                 |
| c                                 | 30.7015(12) Å                               | 20.3605(6) Å                                | 18.7444(13) Å                               |
| a                                 | 90°   | 90°   | 96.095(2)°                                  |
| b                                 | 95.284(2)°                                  | 93.1690(10)°                                | 90.131(2)°                                  |
| g                                 | 90°   | 90°   | 101.235(2)°                                 |
| Volume                            | 2434.22(16) Å <sup>3</sup>                  | 2536.01(12) Å <sup>3</sup>                  | 1374.45(17) Å <sup>3</sup>                  |
| Z                                 | 4   | 8   | 2   |
| Density (calculated)              | 1.469 Mg/m <sup>3</sup>                     | 1.774 Mg/m <sup>3</sup>                     | 1.556 Mg/m <sup>3</sup>                     |
| Absorption coefficient            | 0.958 mm <sup>-1</sup>                      | 6.263 mm <sup>-1</sup>                      | 1.856 mm <sup>-1</sup>                      |
| F(000)                            | 1108  | 1368  | 668   |
| Theta range for data collection   | 1.33 to 25.60°.                             | 4.35 to 64.20°.                             | 4.75 to 64.87°.                             |
| Reflections collected             | 16173                                       | 10983                                       | 17792                                       |
| Independent reflections           | 4551 [R(int) = 0.0857]                      | 2079 [R(int) = 0.0391]                      | 4556 [R(int) = 0.0368]                      |
| Completeness to theta             | 99.2%                                       | 98.10%                                      | 97.90%                                      |
| Max. and min. transmission        | 0.9102 and 0.7004                           | 0.3530 and 0.3035                           | 0.6541 and 0.6060                           |
| Refinement method                 | Full-matrix least-squares on F <sup>2</sup> | Full-matrix least-squares on F <sup>2</sup> | Full-matrix least-squares on F <sup>2</sup> |
| Data / restraints / parameters    | 4551 / 0 / 298                              | 2079 / 0 / 175                              | 4556 / 0 / 428                              |
| Goodness-of-fit on F <sup>2</sup> | 1.057                                       | 1.059                                       | 1.039                                       |
| Final R indices [I > 2σ(I)]       | R1 = 0.0504, wR2 = 0.1390                   | R1 = 0.0316, wR2 = 0.0823                   | R1 = 0.0403, wR2 = 0.1064                   |
| R indices (all data)              | R1 = 0.0717, wR2 = 0.1493                   | R1 = 0.0324, wR2 = 0.0831                   | R1 = 0.0414, wR2 = 0.1075                   |

### 2.3. Synthesis of 2-(2-(1H-benzo[d]imidazol-2-yl)hydrazono)propan-1-ol (L)

The schematic representation of the synthesis of ligand is given in scheme 1. First, 2-bromobenzimidazole was obtained from 2-mercaptobenzimidazole by the reported method [24]. In the next step, 2-bromobenzimidazole (1.97 g, 10 mmol) was refluxed in 20.0 mL of 80% hydrazine hydrate solution, to obtain 2-hydrazinobenzimidazole (1.35 g, Yield : 91%) [25]. Finally, to the magnetically stirred methanolic solution of 2-hydrazinobenzimidazole (1.65 g, 10.0 mmol), hydroxyacetone (0.740 g, 10.0 mmol) in methanol was added dropwise. The mixture was refluxed on a water bath for 1 h. The progress of the reaction was monitored

by TLC. The buff colored precipitate formed was filtered and washed with cold methanol. The solid product was dried *in vacuo* for 4 h.

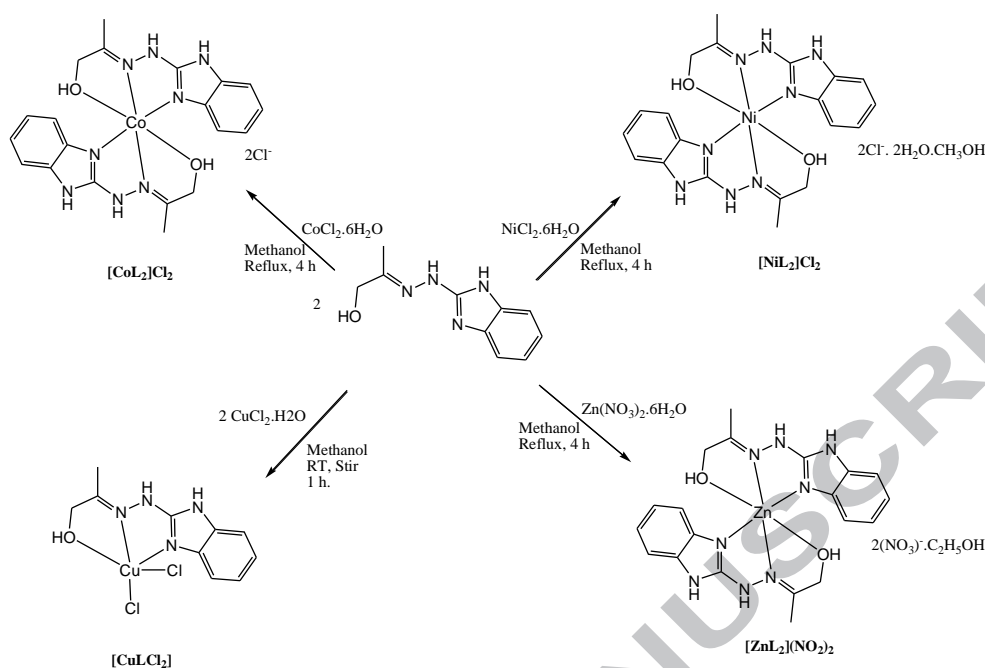
Yield 52%; m.p. 210°C; Color: buff. Anal. Calc. for C<sub>10</sub>H<sub>12</sub>N<sub>4</sub>O (%) : C, 58.81; H, 5.92; N, 27.43; O, 7.83. Found for L (%) : 58.3; H, 6.2; N, 27.8; O, 7.7. FTIR (in cm<sup>-1</sup>):  $\nu(\text{C}=\text{N})$  1637; benzimidazole ring,  $\nu(\text{C}=\text{N})$  1578; hydrazine,  $\nu(\text{NH})$  3246 and 3111;  $\nu(\text{O}-\text{H})$  3440;  $\nu(\text{C}-\text{O})$  1029. <sup>1</sup>H NMR (400 MHz, DMSO-*d*<sub>6</sub>)  $\delta$ : 11.36 (s, 1H, N<sub>2</sub>H), 10.22 (s, 1H, N<sub>3</sub>H), 7.17 (d, 2H, J = 8Hz, C<sub>6</sub>H and C<sub>9</sub>H), 6.99 (s, 2H, C<sub>7</sub>H and C<sub>8</sub>H), 4.88 (t, 1H, J = 5.6Hz, OH), 4.04 (d, 2H, J = 5.6Hz, C<sub>1</sub>H<sub>2</sub>), 1.88 (s, 3H, C<sub>3</sub>H<sub>3</sub>). <sup>13</sup>C NMR (100 MHz, DMSO-*d*<sub>6</sub>)  $\delta$ : 154.92 (C<sub>2</sub>), 150.76 (C<sub>4</sub>), 142.68, 133.54, 120.68, 119.34, 115.28, 109.67 (C<sub>5</sub>-C<sub>10</sub>, Ph), 65.62 (C<sub>1</sub>), 13.86 (C<sub>3</sub>). EI-MS (m/z): 204 ([M]<sup>+</sup>).



Scheme 1 Synthesis of ligand

## 2.4. Syntheses of metal complexes

Schematic representation of the synthesis of the complexes is given in scheme 2. Co(II) and Ni(II) complexes were obtained by refluxing the respective hexa hydrated metal chlorides (0.119 g, 0.500 mmol) with the methanolic solution of ligand (0.204 g, 1.00 mmol) for 4 h. The crystalline product was obtained by evaporating the solvent under reduced pressure. Single crystals were obtained by evaporating the methanolic solution of respective complexes. To the methanolic solution of ligand (0.204 g, 1.00 mmol), a methanolic solution of CuCl<sub>2</sub>·2H<sub>2</sub>O (0.171 g, 1.00 mmol) was added dropwise and the resulting suspension was stirred for 1 h at room temperature. The brown precipitate obtained was filtered off, washed with cold methanol and dried *in vacuo*. Tiny single crystals suitable for X-ray diffraction were obtained by slow evaporation of the filtrate. Whereas the Zn(II) complex was obtained by refluxing Zn(NO<sub>3</sub>)<sub>2</sub>·6H<sub>2</sub>O (0.149 g, 0.500 mmol) with the methanolic solution of ligand (0.204 g, 1.00 mmol) for 4 h. The white product was filtered and washed with methanol. Single crystals were obtained by evaporating the ethanolic solution of the complex.



#### 2.4.1. [CoL<sub>2</sub>]Cl<sub>2</sub>

Color: Faint pink, Yield: 55%. Anal. Calc. for C<sub>20</sub>H<sub>24</sub>Cl<sub>2</sub>CoN<sub>8</sub>O<sub>2</sub>: C, 44.62; H, 4.49; Cl, 13.17; Co, 10.95; N, 20.82; O, 5.94. Found: C, 44.2; H, 4.6; Cl, 12.9; Co, 11; N, 21.7; O, 6.2.  $\lambda_{\max}$  (nm)  $\epsilon_M$  (L M<sup>-1</sup> cm<sup>-1</sup>): 466 (130), 798 (16), 921 (10) (d-d transitions). IR (cm<sup>-1</sup>):  $\nu$ (NH) 3150;  $\nu$ (C=N) 1584,  $\nu$ (O-H) 3440 ;  $\nu$ (C-O) 1060. ESI-MS (positive mode m/z) 466 ([CoL<sub>2</sub>-H]<sup>+</sup>), 233.5 ([CoL<sub>2</sub>]<sup>2+</sup>). Molar conductivity (Ohm<sup>-1</sup> cm<sup>2</sup> mol<sup>-1</sup>): 210.

#### 2.4.2. [NiL<sub>2</sub>]Cl<sub>2</sub>

Color: Blue, Yield: 62%. Anal. Calc. for C<sub>21</sub>H<sub>32</sub>Cl<sub>2</sub>N<sub>8</sub>NiO<sub>5</sub>: C, 41.61; H, 5.32; Cl, 11.70; N, 18.49; Ni, 9.68; O, 13.20. Found: C, 41.1; H, 5.5; Cl, 12.1; N, 18.6; Ni, 9.9; O, 12.8.  $\lambda_{\max}$  (nm)  $\epsilon_M$  (L M<sup>-1</sup> cm<sup>-1</sup>): 453 (44), 601(14), 924 (25) (d-d transitions). IR (cm<sup>-1</sup>):  $\nu$ (NH) 3160;  $\nu$ (C=N) 1584,  $\nu$ (O-H) 3440 ;  $\nu$ (C-O) 1053. ESI-MS (positive mode m/z) 465 ([NiL<sub>2</sub>-H]<sup>+</sup>), 233 ([NiL<sub>2</sub>]<sup>2+</sup>). Molar conductivity (Ohm<sup>-1</sup> cm<sup>2</sup> mol<sup>-1</sup>): 225.

#### 2.4.3. [CuLCl<sub>2</sub>]

Color: Brown, Yield: 43%. Anal. Calc. for C<sub>10</sub>H<sub>12</sub>Cl<sub>2</sub>CuN<sub>4</sub>O: C, 35.46; H, 3.57; Cl, 20.94; Cu, 18.76; N, 16.54; O, 4.72. Found: C, 35.6; H, 3.3; Cl, 21; Cu, 18.2; N, 16.7; O, 5.2.  $\lambda_{\max}$  (nm)  $\epsilon_M$  (L M<sup>-1</sup> cm<sup>-1</sup>): 757 (72) (d-d transition). IR (cm<sup>-1</sup>):  $\nu$ (NH) 3164 ;  $\nu$ (C=N) 1612,  $\nu$ (O-H) 3440 ;  $\nu$ (C-O) 1047. ESI-MS (positive mode m/z) 266 ([CuL-2Cl-H]<sup>+</sup>). Molar conductivity (Ohm<sup>-1</sup> cm<sup>2</sup> mol<sup>-1</sup>): 35.

#### 2.4.4. [ZnL<sub>2</sub>](NO<sub>3</sub>)<sub>2</sub>

Color: White, Yield: 65%. Anal. Calc. for C<sub>22</sub>H<sub>30</sub>N<sub>10</sub>O<sub>9</sub>Zn: C, 41.04; H, 4.70; N, 21.75; O, 22.36; Zn, 10.15. Found: C, 40.5; H, 5.1; N, 21.3; O, 22.95; Zn, 10.15. IR (cm<sup>-1</sup>): ν(NH) 3207; ν(C=N) 1633, ν(O-H) 3440 ; ν(C-O) 1070; ν (N-O) 1384. ESI-MS (positive mode m/z) 472 ([M-2(NO<sub>3</sub>)]<sup>+</sup>). <sup>1</sup>H NMR (DMSO-*d*<sub>6</sub>) δ: 12 (b, 4H, N<sub>2</sub>H and N<sub>3</sub>H ), 7.33-7.02 ( b, C<sub>6</sub>-C<sub>9</sub>H, 8H), 4.31 (s, 4H, C<sub>1</sub>H<sub>2</sub>), 3.40 (q, 2H, J = 6.8 Hz, ethanol), 3.13 (s, 2H, OH), 2.16 (s, 6H, C<sub>3</sub>H<sub>3</sub>), 1.02 (t, 3H, J = 6.8 Hz, ethanol). 472 ([ZnL<sub>2</sub>-H]). Molar conductivity (Ohm<sup>-1</sup> cm<sup>2</sup> mol<sup>-1</sup>): 240.

#### 2.5. Growth inhibitory activity of H37 RV using MABA[26]

The *in vitro* growth inhibitory activity of compounds were assessed against *M. TB* H37Rv genome using microplate Alamar Blue assay (MABA). MABA is sensitive, rapid, inexpensive, nonradiometric, non-toxic and offers the potential for screening, with or without analytical instrumentation for a large number of antimicrobial compounds against slow-growing mycobacteria such as H37Rv, H37Ra, and *M. avium* [27]. Overall, MICs determined either visually or fluorometrically in MABA were highly correlated with those determined in the BACTEC 460 system. Briefly, 200 μL of sterile deionized water was added to all outer perimeter wells of sterile 96 wells plate to minimize the evaporation of medium in the test wells during incubation. The 96 wells plate was loaded with 100 μL of the Middlebrook 7H9 broth. Serial dilution of compounds was made directly on the plate. The final drug concentrations tested were 100 to 0.2 μg/mL. Parafilm-covered sealed plates were covered and incubated at 37 °C for five days. Since H37Rv is categorized as a slow growing bacteria, five days long incubation period is necessary to overcome the imposed limitation in MABA. After the incubation period, 25 μL of freshly prepared 1:1 mixture of Almar Blue reagent and 10% tween 80 was added to the plate. Again the plate was incubated for 24 h. A blue color in the well was scored as no bacterial growth, and pink color was interpreted as growth. The MIC was defined as lowest drug concentration which prevented the color change from blue to pink.

#### 2.6. Growth inhibitory activity of other microbial strains[28]

The MIC values of all synthesized compounds for the growth inhibition of four different microbial genomes *S. aureus*, *E.coli*, *A.niger* and *C.albicans* were determined in HIMEDIA M210 Brain heart infusion broth (BHI). Brain Heart Infusion broth, which is used for the propagation of pathogenic cocci and other fastidious organisms associated with allied pathological investigations had the following composition.

Ingredients in g/L. Calf brain, infusion from, 200.00; Beef heart infusion from, 250.00; Proteose peptone, 10.00; Dextrose, 2.00; Sodium chloride, 5.00; Disodium phosphate, 2.50. And the final pH (at 25<sup>o</sup>C) was 7.4+/-0.2.

9 dilutions of each drug were done with BHI for MIC determination. In the initial tube, 20  $\mu\text{L}$  of the drug was added to the 380  $\mu\text{L}$  of BHI broth. For dilutions, 200  $\mu\text{L}$  of BHI broth was added into the next 9 tubes separately. Then from the initial tube 200  $\mu\text{L}$  was transferred to the first tube containing 200  $\mu\text{L}$  of BHI broth. This was considered as  $10^{-1}$  dilution. From  $10^{-1}$  diluted tube, 200  $\mu\text{L}$  was transferred to the second tube to make  $10^{-2}$  dilution. The serial dilution was repeated up to  $10^{-9}$  dilution for each drug. From the maintained stock cultures of required organisms, 5  $\mu\text{L}$  was taken and added into 2 mL of BHI broth. In each serially diluted tube, 200  $\mu\text{L}$  of above culture suspension was added. The tubes were incubated for 24 hours and observed for turbidity.

### 2.7. Molecular modeling/Docking studies

The 3D structure of the organic ligand was generated using the SKETCH module of SYBYL package (Tripos Associates, St. Louis, MO, USA). The geometry optimization of the organic ligand was done with the help of standard Tripos force field [29] using a distance dependent-dielectric function, energy gradient of 0.001 kcal/ mol and Gasteiger-Huckel as the electrostatics. Conformations were minimized with Tripos force field and atomic charges were calculated using Gasteiger-Huckel method. Whereas the coordinates of all the complexes were taken from their respective crystal structure as a CIF file and were converted to the PDB format using Mercury software [30].

Molecular docking was used to clarify the binding mode of the compounds to provide straightforward information for further structural optimization. Surflex-Dock that adopted an empirical scoring function and a patented searching engine [31, 32] was employed for molecular docking. The target protein structure was obtained from the crystal structure of *Mycobacterium tuberculosis* enoyl reductase complexed with *N*-(5-chloro-2-methylphenyl)-1-cyclohexyl-5-oxopyrrolidine-3-carboxamide (PDB ID: 4U0K)[33] at a resolution of 1.9  $\text{\AA}$  which was extracted from the Brookhaven Protein Database (PDB <http://www.rcsb.org/pdb>). The proteins were prepared for docking by adding polar hydrogen atom with Gasteiger-Huckel charges and water molecules were removed. And other miscellaneous parameters were assigned with the default values given by the software.

## 3. Results and discussion

### 3.1. Synthesis

The ligand precursor 2-hydrazinobenzimidazole has been prepared by a new efficient synthetic route, which involved the conversion of 2-mercaptobenzimidazole into 2-bromobenzimidazole. Synthesis of the newly designed ligand along with its metal complexes has been described in experimental section.

### 3.2. Spectral characterization

In the IR spectra (SI-S.1), the free ligand shows a relatively sharp band at  $3440\text{ cm}^{-1}$ . This is assignable to  $\nu(\text{O-H})$  of the ligand where the hydrogen atom of the hydroxyl group is hydrogen bonded [34]. This band has significantly broadened in all the complexes, indicating the coordination of oxygen atom without deprotonation. The band at  $1020\text{ cm}^{-1}$ , which is due to  $\nu(\text{C-O})$  has shown a significant positive shift in all the complexes due to the coordination of oxygen. The ligand has shown a sharp intense band at  $1637\text{ cm}^{-1}$  and is assigned to the  $\nu(\text{C=N})$  of imine. The sharp intense band at  $1578\text{ cm}^{-1}$  is assignable to  $\nu(\text{C=N})$  of benzimidazole ring. In the complexes, these two bands have given a coupled vibration with decreased intensity and significant negative shift, indicating the coordination of azomethine as well as ring nitrogen [35]. A peak at  $3246\text{ cm}^{-1}$  in the ligand, which is due to  $\nu(\text{N-H})$ , has suffered from low energy shift in all the complexes [36]. This observation again confirms the coordination of azomethine nitrogen. The very sharp band at  $1384\text{ cm}^{-1}$  in the case of  $[\text{ZnL}_2](\text{NO}_3)_2$  is characteristic of nitrate counterions [37]. The similarity pattern observed in the spectra of  $[\text{CoL}_2]\text{Cl}_2$  and  $[\text{NiL}_2]\text{Cl}_2$  suggests the similarity in structures. Further, the appearance of new bands in the region of  $520\text{-}560$  and  $400\text{-}490\text{ cm}^{-1}$  are evidencing the newly formed M-N and M-O bonds in all the complexes [38]. Conclusively this suggests NNO, tridentate behavior of the ligand.

$^1\text{H}$  NMR studies have been carried out for the ligand and diamagnetic zinc complex in the region of  $0\text{-}16\ \delta$  ppm. The spectrum of L (SI-S.2) has shown two broad down field singlets. The broad singlet at  $11.36$  ppm is due to hydrogen of ring nitrogen whereas the other broad singlet at  $10.22$  ppm is assignable to hydrazine N-H [39]. In the  $^1\text{H}$  NMR of the  $[\text{ZnL}_2](\text{NO}_3)_2$  (SI-S.3), these two peaks have merged and given a broad peak around  $12$  ppm. A triplet at  $4.88$  ppm is due to the hydroxyl group, which has coupled with methylene protons. Coordination of hydroxyl group to the metal center has resulted in the downfield shift of this peak to  $3.13$  ppm. In addition, coordination has also interrupted the possible coupling. In the ligand, methylene protons have resonated at  $4.04$  ppm as a doublet. Deshielding of this to  $4.30$  ppm in the complex, reasonably accounts the shielding of coordinated oxygen atom [40]. The singlet at  $1.88$  ppm, which is due to the methyl group of the ligand has shifted to  $2.15$  ppm in the complex. In ligand as well as in complex, the four aromatic protons have resonated in two sets in the expected aromatic region. Triplet at  $1.015$  and quartet centered at  $3.40$ , undoubtedly account for the ethanol solvation in the complex.

The electronic spectra of the ligand, as well as complexes, were recorded in DMF solvent. The strong absorption in the range of  $250\text{-}280\text{ nm}$  is ascribed to intra-ligand  $\pi \rightarrow \pi^*$  transitions. The band has remained almost unchanged in the complexes. The  $n \rightarrow \pi^*$  transition of azomethine functionality is observed between  $300\text{-}350\text{ nm}$  and has suffered bathochromic

shift upon complexation. This is an indication of coordination of imine nitrogen to the metal ions.

The  $[\text{CoL}_2]\text{Cl}_2$  has shown its lowest energy transition around 921nm which is assignable to  ${}^4\text{T}_{1g} \rightarrow {}^4\text{T}_{2g}(\nu_1)$ . The other two transitions observed around 798 and 453 nm are consistent with the energies of,  ${}^4\text{T}_{1g} \rightarrow {}^4\text{A}_{2g}(\nu_2)$  and  ${}^4\text{T}_{1g} \rightarrow {}^4\text{T}_{1g}(\text{P})(\nu_3)$ , octahedral transitions for the  $[\text{CoL}_2]\text{Cl}_2$ . The d-d transitions in  $[\text{NiL}_2]\text{Cl}_2$  are observed around 924, 601 and 453 nm. These are assignable to  ${}^3\text{A}_{2g} \rightarrow {}^3\text{T}_{2g}(\nu_1)$ ,  ${}^3\text{A}_{2g} \rightarrow {}^3\text{T}_{1g}(\nu_2)$  and  ${}^3\text{A}_{2g} \rightarrow {}^3\text{T}_{1g}(\text{P})(\nu_3)$  transitions, which are in support of octahedral geometry of the complex. Absorption spectrum of copper complex has given a *d-d* electronic band at 761 nm. Absorptions in this region are typical of species with square pyramidal geometry around the Cu(II) ions [41].

### 3.3. Mass fragmentation

The EI mass spectrum of the L (SI-S.5) has shown the molecular ion peak  $[\text{M}]^+$  at  $m/z$  204. Further, the intense peak at 173, is due to the loss of a  $\text{CH}_2\text{OH}$  fragment of the ligand indicating the ease of cleavage of this C-C bond. The ESI mass spectra of all the complexes have shown several peaks due to the molecular cations of the various fragments formed during electrospray ionization [35]. The intense peak at 205, in all the complexes, is due to the ligand fragment  $[\text{L}+\text{H}]^+$ . The ESI-MS of  $[\text{NiL}_2]\text{Cl}_2$  has shown a peak at 465, corresponding to  $[\text{NiL}_2\text{-H}]^+$ ; and the base peak at 233, corresponding exactly to the  $m/z$  of  $[\text{NiL}_2]^{2+}$ . Similarly the intense peaks at 466 and 233.5 in  $[\text{CoL}_2]\text{Cl}_2$  are attributed to  $[\text{CoL}_2\text{-H}]^+$  and  $[\text{CoL}_2]^{2+}$  respectively. The peak at 119 in this complex is due to the protonated benzimidazole fragment. ESI-MS of  $[\text{ZnL}_2](\text{NO}_3)_2$  has given a peak at 472, due to the  $[\text{ZnL}_2\text{-H}]^+$ . In  $[\text{CuLCl}_2]$ , in addition to the peak at 266 due to  $[\text{CuL-2Cl-H}]^+$ , the base peak is observed at  $m/z$  307. This accounts for the mass of the species formed by the loss of  $\text{CH}_2\text{OH}$  fragment from the molecule and confirms the ascribed ligand to metal ratio.

### 3.4. Thermal analysis

All the complexes were studied for TG and DT analysis over the temperature range of 25-1000<sup>o</sup>C under nitrogen atmosphere. The thermal decomposition pattern of  $[\text{CuLCl}_2]$  and  $[\text{ZnL}_2](\text{NO}_3)_2$  (SI-Fig.1&2) are dealt in detail.

$[\text{CuLCl}_2]$  has remained thermally stable without any loss of weight up to a temperature of 160<sup>o</sup>C, showing the absence of any lattice held molecules. The weight loss of about 9.3% (Calc. 9.4%) in the range of 160-190<sup>o</sup>C is due to the loss of a methanol fragment of the ligand. This is clearly evidenced in DTA curve in the form of an exothermic peak at 185<sup>o</sup>C. The remaining part of the ligand has decomposed gradually with the increase in temperature.

The initial weight loss of about 7% (Calc.7.1%) in  $[\text{ZnL}_2](\text{NO}_3)_2$  is due to the loss of an ethanol molecule. Further in the temperature range of 228-310 $^{\circ}\text{C}$ , the complex has lost about 30% (Calc. 29.2%) of its weight which is due to the combined loss of two nitrate counter-ions along with 2 methanol fragments of the ligand. This process is further supported by exothermic peaks in DTA curve at 237 and 279 $^{\circ}\text{C}$ . Above 310 $^{\circ}\text{C}$  the complex has gradually lost its weight due to the decomposition of ligand moiety.

The TG and DT analytical data of  $[\text{CoL}_2]\text{Cl}_2$  and  $[\text{NiL}_2]\text{Cl}_2$  are in good agreement with ascribed structures.

### 3.4. Crystal structures

Single crystals of all the complexes suitable for X-ray diffraction studies were grown by slow evaporation technique. The structures of  $[\text{CoL}_2]\text{Cl}_2$ ,  $[\text{CuLCl}_2]$  and  $[\text{ZnL}_2](\text{NO}_3)_2$  has been studied in detail. Asymmetric units of complexes showing 50% displacement ellipsoids along with the numbering scheme are shown in fig. 1-3. Selected bond distances and bond angles are tabulated in tables 2-5.

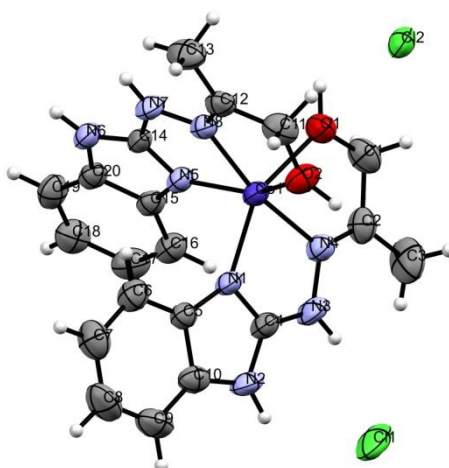


Fig.1 Asymmetric unit of  $[\text{CoL}_2]\text{Cl}_2$  showing 50% displacement ellipsoids.

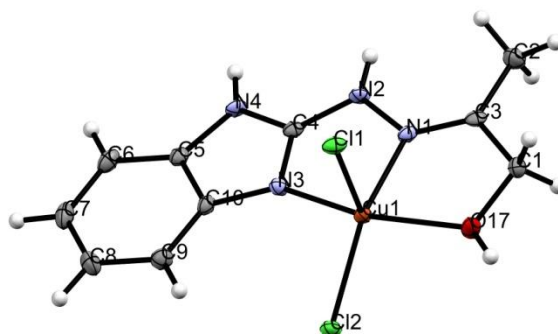


Fig.2 Asymmetric unit of  $[\text{CuLCl}_2]$  showing 50% displacement ellipsoids.

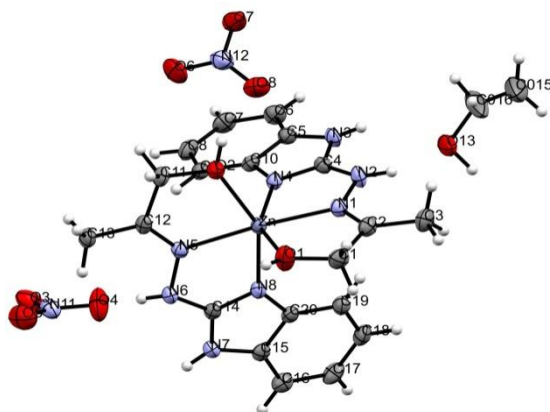


Fig.3 Asymmetric unit of  $[\text{ZnL}_2](\text{NO}_3)_2$  showing 50% displacement ellipsoids.

|                 |            |
|-----------------|------------|
| N(1)-Co(1)      | 2.079(3)   |
| N(4)-Co(1)      | 2.078(3)   |
| N(5)-Co(1)      | 2.096(3)   |
| N(8)-Co(1)      | 2.079(2)   |
| O(1)-Co(1)      | 2.182(2)   |
| O(2)-Co(1)      | 2.151(2)   |
| N(4)-Co(1)-N(8) | 169.30(10) |
| N(4)-Co(1)-N(1) | 77.53(10)  |
| N(8)-Co(1)-N(1) | 112.13(10) |
| N(4)-Co(1)-N(5) | 107.60(10) |
| N(8)-Co(1)-N(5) | 77.18(10)  |
| N(1)-Co(1)-N(5) | 93.50(10)  |
| N(4)-Co(1)-O(2) | 101.48(10) |
| N(8)-Co(1)-O(2) | 74.06(10)  |
| N(1)-Co(1)-O(2) | 93.28(9)   |
| N(5)-Co(1)-O(2) | 150.91(10) |
| N(4)-Co(1)-O(1) | 74.31(10)  |
| N(8)-Co(1)-O(1) | 95.67(9)   |
| N(1)-Co(1)-O(1) | 151.59(10) |
| N(5)-Co(1)-O(1) | 98.51(10)  |
| O(2)-Co(1)-O(1) | 88.63(9)   |

|             |            |
|-------------|------------|
| N(1)-Cu(1)  | 1.989(2)   |
| N(3)-Cu(1)  | 1.959(2)   |
| O(17)-Cu(1) | 2.0226(19) |
| Cl(1)-Cu(1) | 2.5273(6)  |

|                   |           |
|-------------------|-----------|
| Cl(2)-Cu(1)       | 2.2379(7) |
| N(3)-Cu(1)-N(1)   | 80.32(8)  |
| N(3)-Cu(1)-O(17)  | 152.81(8) |
| N(1)-Cu(1)-O(17)  | 76.44(8)  |
| N(3)-Cu(1)-Cl(2)  | 100.90(6) |
| N(1)-Cu(1)-Cl(2)  | 159.80(6) |
| O(17)-Cu(1)-Cl(2) | 96.19(6)  |
| N(3)-Cu(1)-Cl(1)  | 100.22(6) |
| N(1)-Cu(1)-Cl(1)  | 98.56(6)  |
| O(17)-Cu(1)-Cl(1) | 97.04(6)  |
| Cl(2)-Cu(1)-Cl(1) | 101.02(2) |

| Table 4. Selected Bond lengths [ $\text{\AA}$ ] and angles [ $^\circ$ ] for $[\text{ZnL}_2](\text{NO}_3)_2$ |            |
|---|------------|
| Zn-N(4)   | 2.0636(19) |
| Zn-N(8)   | 2.0731(19) |
| Zn-N(5)   | 2.1243(19) |
| Zn-N(1)   | 2.1325(19) |
| Zn-O(1)   | 2.163(2)   |
| Zn-O(2)   | 2.1912(17) |
| N(4)-Zn-N(8)  | 95.69(8)   |
| N(4)-Zn-N(5)  | 114.26(7)  |
| N(8)-Zn-N(5)  | 76.17(7)   |
| N(4)-Zn-N(1)  | 76.63(7)   |
| N(8)-Zn-N(1)  | 105.47(7)  |
| N(5)-Zn-N(1)  | 168.96(8)  |
| N(4)-Zn-O(1)  | 148.39(7)  |
| N(8)-Zn-O(1)  | 95.91(8)   |
| N(5)-Zn-O(1)  | 97.05(7)   |
| N(1)-Zn-O(1)  | 71.96(7)   |
| N(4)-Zn-O(2)  | 94.07(7)   |
| N(8)-Zn-O(2)  | 149.44(7)  |
| N(5)-Zn-O(2)  | 73.41(7)   |
| N(1)-Zn-O(2)  | 104.94(7)  |
| O(1)-Zn-O(2)  | 90.66(7)   |

$[\text{CoL}_2]\text{Cl}_2$  has crystallized in the monoclinic crystal system with  $P2_1/n$  space group. The structure of  $[\text{CoL}_2]\text{Cl}_2$  contains  $[\text{CoL}_2]^{2+}$  cation along with two chloride ions, without any

solvents of crystallization. Each ligand is coordinated to the central metal ion in an NNO tridentate fashion with the benzimidazole-N (N1 and N5), imine-N (N4 and N8) and hydroxyl-O (O1 and O2) as donor atoms. A dihedral angle of  $87.1^\circ$  is observed between the mean planes of two ligands, in which two azomethine nitrogens (N4 and N8) reside *trans* to each other whereas the other two donor sites (N1,N5 and O1,O5) have remained mutually *cis* to each other. The ligand has formed two five-membered chelate rings with the metal center. The O-Co-N and N-Co-N bite angles in case of both the ligands fall around  $74^\circ$  and  $77^\circ$  respectively indicating significant deviation from ideal octahedral geometry in the complex.

The complex structure is stabilized by hydrogen bonding interactions between chloride ions and the complex cations as depicted in the fig. 4. The first chloride (Cl1) ion is hydrogen bonded to N-H hydrogens of benzimidazole ring and N-H of hydrazone functionality of the same ligand with a bond distance of 2.56 Å and 2.43 Å respectively. The second chloride ion (Cl2) has involved in hydrogen bonding with the hydroxyl group of the ligand with a bond distance of 2.50 Å. This chloride ion has even made a hydrogen bond with N-H hydrogen of benzimidazole ring with a bond distance of 2.22 Å.

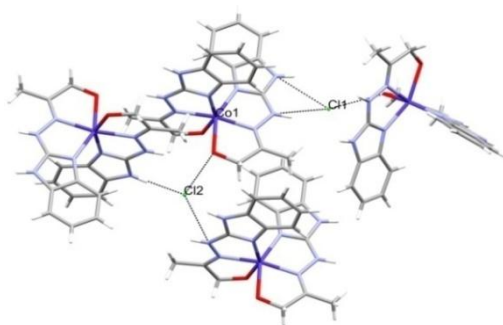


Fig.4 Hydrogen bonding in  $[\text{CoL}_2]\text{Cl}_2$ .

$[\text{CuLCl}_2]$  has crystallized in monoclinic crystal system in the  $C2/c$  space group. The structure of  $[\text{CuLCl}_2]$  contains a neutral complex molecule without any solvents of crystallization. The ligand is coordinated to the central metal ion in an NNO tridentate fashion with the benzimidazole-N (N3), imine-N (N1) and hydroxyl-O (O17) as donor atoms. In addition, two chloride ions have coordinated; resulting in a penta coordinated tetragonally distorted square pyramidal complex. The ligand has formed two five-membered chelate rings with the metal center. The bond angles have deviated significantly from  $90^\circ$ , indicating the deviation from ideal square pyramidal geometry. The verified axial (Cu1-Cl1) distance 2.52 Å is considerably longer than the basal (Cu1-Cl2) distance 2.23 Å in the structure, as ascertained by Reedijk's  $\tau$  factor of 0.002 [42]. ( $\tau = 0$  for a square pyramid, and  $\tau = 1$  for a trigonal bipyramid) [43].

$[\text{CuLCl}_2]$  is also stabilized by hydrogen bonding interactions of chloride ligand; which has given a layered arrangement of complexes as depicted in fig.5. The equatorial chlorides

(Cl2) and hydroxyl hydrogens of two adjacent molecules of the same layer are involved in hydrogen bonding with a bond distance of 2.21 Å. The axial chlorides (Cl1) have made bonds with 2 adjacent molecules of the next layer, using benzimidazole N-H of one molecule and hydrazide N-H of the other with a bond distance of 2.46 and 2.30 Å respectively.

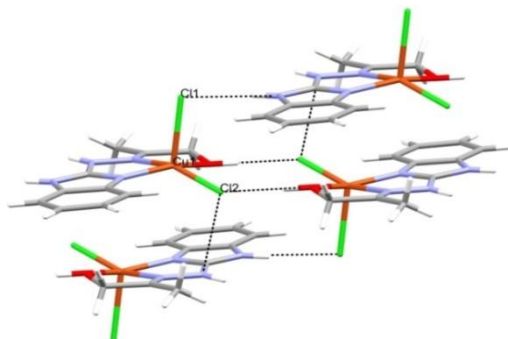


Fig.5 Hydrogen bonding in  $[\text{CuLCL}_2]$ .

$[\text{ZnL}_2](\text{NO}_3)_2$  has crystallized in triclinic crystal system with  $P-1$  space group. The structure of  $[\text{ZnL}_2](\text{NO}_3)_2$  contains  $[\text{ZnL}_2]^{2+}$  cation along with two nitrate ions and an ethanol molecule as solvent of crystallization. The coordination behaviour and geometrical aspects of the  $[\text{ZnL}_2](\text{NO}_3)_2$  resembles with that of  $[\text{CoL}_2]\text{Cl}_2$ .

$[\text{ZnL}_2](\text{NO}_3)_2$  is also stabilized by several hydrogen bonding interactions among complex cation, nitrate ions and ethanol. First nitrate ion (N11) is hydrogen bonded to hydrazide N-H of one molecule and ring N-H of the other molecule with the help of two different oxygen atoms. The corresponding bond distances are 2.09 and 2.26 Å respectively. Simultaneously these two oxygens are even interacting with the hydroxyl hydrogens of the third molecule, with the bond distances of 2.03 and 2.09 Å respectively. Whereas in the second nitrate ion (N12), one oxygen is hydrogen bonded to hydroxyl hydrogen of one molecule and with the other oxygen it is interacting with benzimidazole N-H and hydroxyl hydrogen of ethanol. The bond distances are 1.89, 2.26 and 1.86 Å respectively. The oxygen (O13) of ethanol is accepting two bonds with hydrazide and benzimidazole N-Hs of the same ligand, at a distance of 1.86 and 2.59 Å respectively.

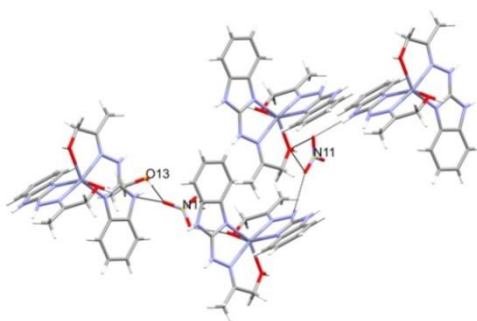


Fig.6 Hydrogen bonding in  $[\text{ZnL}_2](\text{NO}_3)_2$

### 3.5. Cyclic voltammetry and conductivity

All complexes were studied for their electrochemical behavior by cyclic voltammetric experiments at room temperature. The experiments were carried out in oxygen-free conditions in the potential range of -1.00 to +1.00 V, using glassy carbon working electrode, a platinum counter electrode and Ag/Ag<sup>+</sup> reference electrode in DMF with varied scan rates. The copper complex is found to be electrochemically active in the scanned range whereas the other complexes are found to be electrochemically innocent. The voltammogram of copper complex is given in fig.7. The copper complex has exhibited redox process corresponding to Cu(II)/Cu(I) couple with a cathodic peak at  $E_{pc} = 0.42$  V, corresponding to Cu(II)/Cu(I) and respective anodic peak for Cu(I)/Cu(II) at  $E_{pa} = 0.51$  V. The value of  $\Delta E_p$  is more than 59 mV, indicating quasi-reversible redox process. The peak potential dependency on scan rates and value ( $\sim 1$ ) for  $I_a/I_b$  (ratio of oxidative to reductive peak currents) indicates simple one electron transfer [44].

The molar conductivity values for  $[\text{CoL}_2]\text{Cl}_2$ ,  $[\text{NiL}_2]\text{Cl}_2$  and  $[\text{ZnL}_2](\text{NO}_3)_2$  are above 200  $\text{Ohm}^{-1} \text{cm}^2 \text{mol}^{-1}$  indicating the 1:2 electrolytic nature of the complex[40], while  $[\text{CuLCl}_2]$  being non-electrolytic in nature.

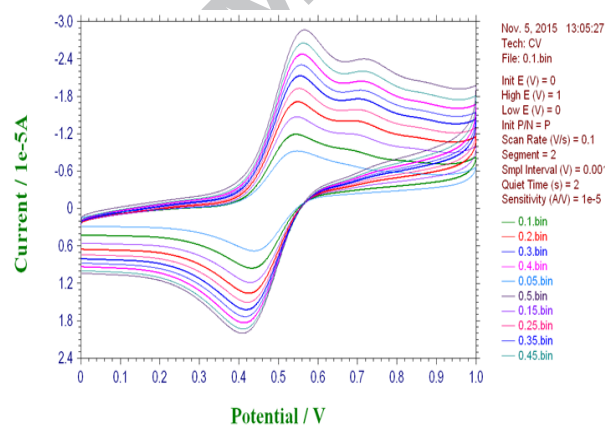


Fig.7. Voltammogram of  $[\text{CuLCl}_2]$

### 3.6. In vitro growth inhibition of H37Rv

The drug-susceptible strain of *M. tuberculosis*, H37Rv[45] was used to determine the growth inhibitory activity of ligand, complexes as well as streptomycin using microplate Alamar blue assay (MABA). Results are tabulated in table 5.

| Sample                      | <i>M. tuberculosis</i><br>(H37Rv) | <i>S. aureus</i> | <i>E. coli</i> | <i>A. niger</i> | <i>C. albicans</i> |
|-----------------------------|-----------------------------------|------------------|----------------|-----------------|--------------------|
| $[\text{CoL}_2]\text{Cl}_2$ | 6.25                              | 25               | 50             | 50              | 50                 |
| $[\text{NiL}_2]\text{Cl}_2$ | 50                                | 25               | 50             | 50              | 50                 |
| $[\text{CuLCl}_2]$          | 6.25                              | 12.5             | 25             | 50              | 50                 |

|  |      |      |    |    |    |
|--|------|------|----|----|----|
| [ZnL <sub>2</sub> ](NO <sub>3</sub> ) <sub>2</sub> | 25   | 25   | 50 | 25 | 25 |
| <b>L</b>   | 25   | 1.6  | 50 | 50 | 50 |
| <b>Streptomycin</b>                                | 6.25 | 3.12 | 25 | -  | -  |
| <b>Fluconazole</b>                                 | -    | -    | -  | 8  | 16 |

The efficacies of all synthesized compounds along with the standard streptomycin/Fluconazole for the growth inhibition of four different microbes of the wide taxonomical range were tested using the microbial strains of *Staphylococcus aureus*, *Escherichia coli*, *Aspergillus Niger* and *Candida albicans*. Results are tabulated in table 3. The results though unexpected, were significant due to ceased growth inhibition of tested microbes in comparison with H37Rv. The MIC values of new complexes for *S.aureus* falls in the range of 25-12.5 µg/mL, whereas for *E.Coli* the MIC value is found to be ranging up to 50µg/mL. These values are sufficiently higher than the standard drug streptomycin which inhibits the *S. aureus* growth, even at 3.12µg/mL. The MIC values for tested fungal strains are beyond 25µg/mL, which makes the strains resistant towards the tested compounds even at higher concentrations than the standard fluconazole whose MIC is sufficiently low towards tested fungi.

These results are significant in bringing the selectivity towards the growth inhibition of H37Rv by metal insertion. Especially cobalt and copper complexes are found to be selectively active against TB strain H37Rv[46] and have inhibited the growth of the species even at a concentration as low as 6.25 µg/m, while the same being less active against other tested microbes. Notably, this kind of selectivity is not observed in the case of bare ligand or even in the standard drug streptomycin.

The specific differences in the growth inhibiting potencies of the complexes of same ligand system with different metal ions can be explained on the basis of Overtones concept of cell permeability. The Co (II) ion bears lowest dipole moment, which could be related to its excellent activity than other complexes. The decrease in dipole moment eventually reduces polarity and hence increases the lipophilic nature of the complex, favoring the efficient permeation through lipid layer of the microorganism [47]. The ligand was chosen as a design tool to produce mononuclear complexes, with hydrophilic 'cores' and hydrophobic exteriors. Such complexes are water-soluble and capable of facile hydrolysis making such complexes potential pro-drugs, which when coupled with the redox properties of the metals complexed, is a strong approach to new metal-based therapeutics [48].

### 3.7. Molecular modeling/Docking studies

To investigate the mechanism of microbial growth inhibition, the effect of metal ions and detailed intermolecular interactions between the synthesized compounds and microbial target receptors, molecular docking studies were performed on enoyl acyl carrier protein reductase of *M. tuberculosis* H37Rv. This enzyme is one of the key enzymes involved in the mycobacterial fatty acid

elongation cycle and has been validated as an effective antimicrobial target [49]. The binding domain identified to accommodate is large enough to hold the synthesized molecules although these molecules occupy slightly a larger volume. The possibility of larger molecular volumes resulting in low docking scores is due to the fact that the size of the binding pocket being smaller than the molecular volumes. The copper complex possessing relatively small volume due to its geometry, coordinated halides and single ligand has shown more binding efficiency towards the target site. The predicted binding energies of the compounds are listed in table 6.

| Compounds  | C Score | Crash Score | Polar Score | D Score  | PMF Score | G Score | Chem Score |
|--|---------|-------------|-------------|----------|-----------|---------|------------|
| [CoL <sub>2</sub> ]Cl <sub>2</sub>                 | 2.55    | -0.28       | 1.02        | -7019.61 | 30.23     | -99.14  | -19.21     |
| [NiL <sub>2</sub> ]Cl <sub>2</sub>                 | 2.22    | -0.38       | 0.70        | -5383.20 | 0.79      | -116.64 | -19.33     |
| [CuL]Cl <sub>2</sub>                               | 3.15    | -0.26       | 3.03        | -2265.29 | -4.63     | -80.64  | -20.02     |
| [ZnL <sub>2</sub> ](NO <sub>3</sub> ) <sub>2</sub> | 2.79    | -0.65       | 0.00        | -6614.84 | 15.63     | -155.34 | -22.31     |
| <b>L</b>   | 2.67    | -0.34       | 2.19        | -1088.59 | -3.02     | -81.47  | -14.54     |

The molecules showed consensus scores in the range of 2.22-3.15, indicating the summary of all forces of interactions between the compounds and protein. [CuLCl<sub>2</sub>] has shown relatively high C (consensus) scores showing the affinity of this molecule in binding the active site of the receptor. Crash-scores are revealing the inappropriate penetration into the binding site. The copper and cobalt complexes which are showing the crash scores close to zero are favorable, while the high negative value in other cases is indicating penetration. The positive value of polar scores is indicating the significant contribution of the polar interactions to the total score. The zero polar score in the case of [ZnL<sub>2</sub>](NO<sub>3</sub>)<sub>2</sub> may be useful for excluding docking results since it makes no significant hydrogen bonds. The high value of D-score in the case of cobalt complex is due to the charge and van der Waals interactions between the protein and the ligand [50]. Further, this is in accordance with the overtones concept of cell permeability, which in turn explains the observed activity of the cobalt complex in comparison with the other complexes. The PMF-scores in the case of complexes indicates more Helmholtz free energies of interactions for protein-molecule atom pairs (Potential of Mean Force, PMF)[51] than in the case of the free ligand. The G-score is showing hydrogen bonding, complex (molecule-protein), and internal energies,[52] while the Chem-score points for H-bonding, lipophilic contact, and rotational entropy, along with an intercept term [53].

The interaction of [CuLCl<sub>2</sub>] with the enzyme is depicted in Fig. 8 and Fig. 9, showing three hydrogen bonding interactions, among which two are raised from the hydroxyl group. The oxygen atom of the hydroxyl group of [CuLCl<sub>2</sub>] is involved in H-bonding interaction with the hydrogen of threonine 386 (H-O---H-THR; 2.30 Å) and the hydrogen atom of hydroxyl

group makes an interaction with the oxygen atom of valine 373 (O-H ----O-VAL373; 2.05 Å). The third hydrogen bonding interaction has raised from the hydrazide N-H with the oxygen atom of threonine 386 (N-H----O-THR386; 1.73 Å). Fig.10 and 11 depict the two interactions of the ligand with the active site of the enzyme. The hydrogen atom of the hydroxyl group of ligand has interacted with valine 371 (O-H----O-VAL371; 1.91 Å) and the benzimidazole ring-N is hydrogen bonded to the oxygen atom of threonine 386 (N-H----H-THR386; 2.01 Å).

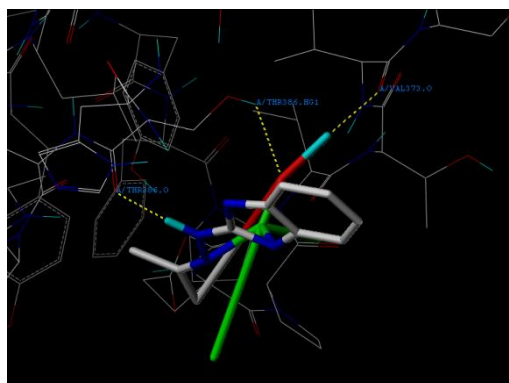


Fig.8 Docking poses of the  $[CuLCl_2]$  with amino acid residues at the active site of the enzyme.

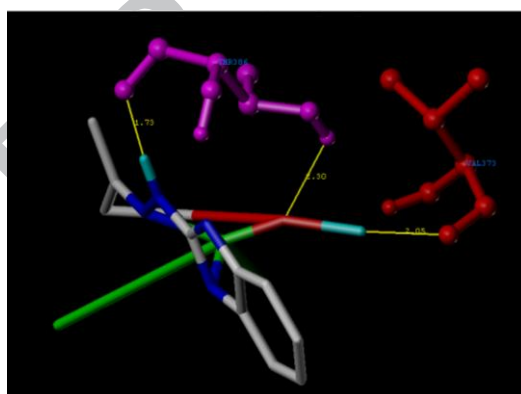


Fig.9 Docking poses of the  $[CuLCl_2]$  showing the distance between the amino acids with the interacted atoms.

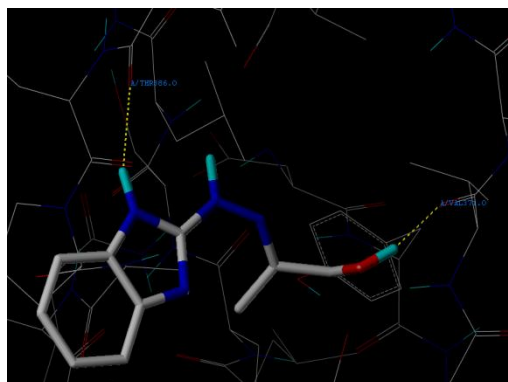


Fig.10 Docking poses of the ligand with amino acid residues at the active site of the enzyme.

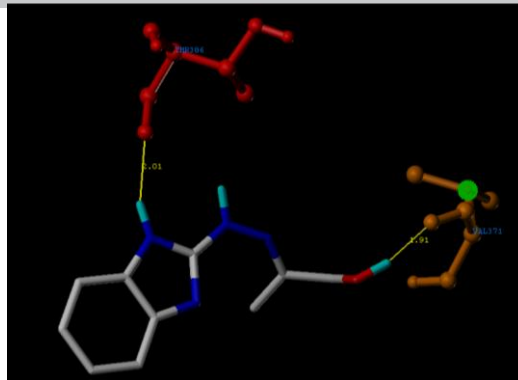


Fig.11 Docking poses of the ligand showing the distance between the amino acids with the interacted atoms.

#### 4. Conclusions

In the present work, a newly designed benzimidazole based Schiff base ligand 2-(2-(1H-benzo[d]imidazol-2-yl)hydrazono)propan-1-ol has been synthesized via 2-hydrazinobenzimidazole. The organic motif binds the dipositive metal centers in NNO tridentate mode through benzimidazole-N, azomethine-N and hydroxyl-O atoms respectively. Analytical and spectroscopic data for the metal complexes indicate a 1:1 (M:L) stoichiometry for copper and 1:2 for the remaining complexes. Except the non-electrolytic copper complex, all other complexes are found to be 1:2 electrolytes. Co(II), Cu(II) and Zn(II) complexes have crystallized in  $P2_1/n$ ,  $C2/c$  and  $P-1$  space groups respectively. SC-XRD structures of Co(II), and Zn(II) complexes reveal that the metal center is coordinated in an  $N_4O_2$  core by a tridentate ligand in a meridional fashion, and adopts a distorted octahedral geometry. Whereas the Cu(II) complex has adopted distorted square pyramidal geometry. The complexes are stabilized by intermolecular hydrogen bonding interactions. The copper complex, was electrochemically active in the working potential range, showing quasi-reversible redox system. In addition, the ESI-mass and thermal analysis of the copper complex are showing the presence of an activated C-C bond, which is of particular interest in catalysis, for future studies. Cobalt as well as copper complexes have emerged to be potent growth inhibitors of TB strain H37Rv and have inhibited the growth of the species even at a concentration as low as 6.25  $\mu\text{g/mL}$ . The MIC value for other microbial strains is beyond 25  $\mu\text{g/mL}$  which makes the strains resistant towards the tested compounds even at higher concentrations, bringing selectivity towards the growth inhibition of H37Rv by metal insertion. This result would create a future interest in bringing the metal based target specificity of existing drugs. Molecular modeling of the compounds with the molecular target site of enoyl acyl carrier protein reductase of *M. tuberculosis* H37Rv revealed that the molecules fit in the active site of the receptor. Consensus scores for the complexes are in the range of 2.22-3.15. Copper complex which emerged with high C-score of 3.15 is shown to be a better antitubercular agent than bare parent organic motif. This docking result of copper complex is in agreement with the observed MIC value.

## Appendix A. Supplementary data

CCDC 1443163, 1459338 and 1454181 contains the supplementary crystallographic data for  $[\text{CoL}_2]\text{Cl}_2$ ,  $[\text{CuLCl}_2]$  and  $[\text{ZnL}_2](\text{NO}_3)_2$ . These data can be obtained free of charge via <http://www.ccdc.cam.ac.uk/conts/retrieving.html>, or from the Cambridge Crystallographic Data Centre, 12 Union Road, Cambridge CB2 1EZ, UK; fax: (+44) 1223-336-033; or e-mail: [deposit@ccdc.cam.ac.uk](mailto:deposit@ccdc.cam.ac.uk).

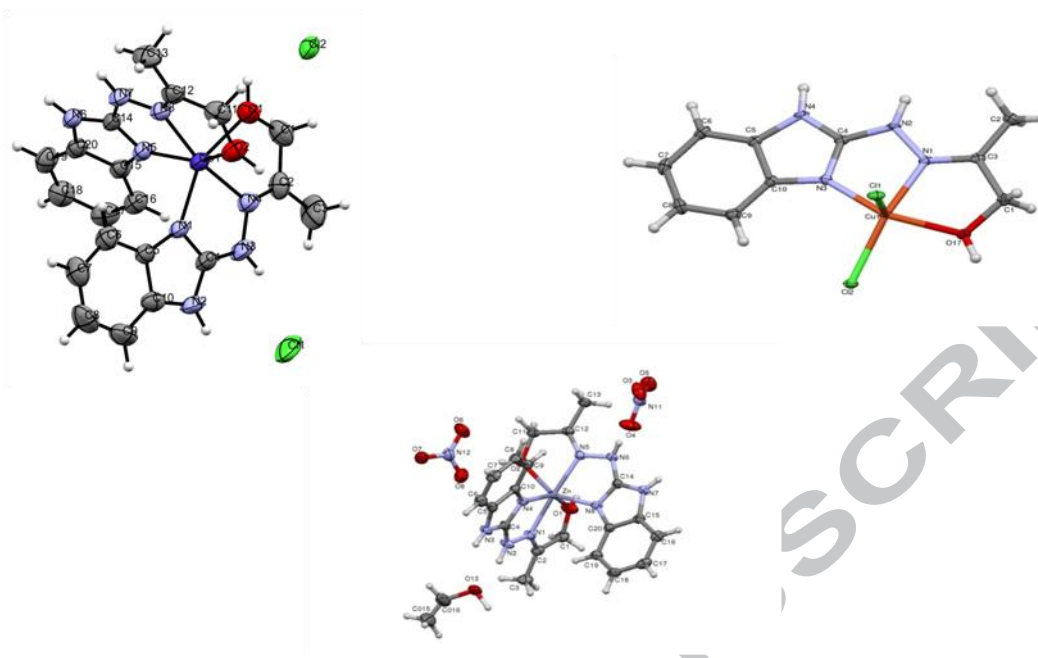
## Acknowledgements

The authors thank USIC, Karnatak University, Dharwad, for providing spectral facilities. Recording of ESI-mass spectra from CDRI-Lucknow is greatly acknowledged. SC-XRD data collected from IOE-University of Mysore is also greatly acknowledged. One of the authors (Vinayak Kamat) is thankful to Department of Science & Technology for providing financial assistance under INSPIRE fellowship program and to UGC-New Delhi for JRF.

## References

- [1] K.T. Mahmudov, M.N. Kopylovich, A.J.L. Pombeiro, *Coordination Chemistry Reviews* 257 (2013) 1244-1281.
- [2] S. Shit, S. Sen, S. Mitra, D.L. Hughes, *Transition Metal Chemistry* 34 (2009) 269-274.
- [3] P.M. Vimal Kumar, P.K. Radhakrishnan, *Polyhedron* 29 (2010) 2335-2344.
- [4] C.-M. Che, F.-M. Siu, *Current Opinion in Chemical Biology* 14 (2010) 255-261.
- [5] C.X. Zhang, S.J. Lippard, *Current Opinion in Chemical Biology* 7 (2003) 481-489.
- [6] K. Irena, B. Stefan, *Current Medicinal Chemistry* 20 (2013) 4508-4539.
- [7] D. C. Crans, A. D. Keramidis, S. S. Amin, O. P. Anderson, S. M. Miller, *Journal of the Chemical Society, Dalton Transactions* (1997) 2799-2812.
- [8] D.C. Crans, *The Journal of Organic Chemistry* 80 (2015) 11899-11915.
- [9] J.C. Pessoa, S. Etcheverry, D. Gambino, *Coordination Chemistry Reviews* 301-302 (2015) 24-48.
- [10] C. Santini, M. Pellei, V. Gandin, M. Porchia, F. Tisato, C. Marzano, *Chemical Reviews* 114 (2014) 815-862.
- [11] Z.H. Chohan, C.T. Supuran, A. Scozzafava, *Journal of Enzyme Inhibition and Medicinal Chemistry* 19 (2004) 79-84.
- [12] J. Joseph, K. Nagashri, G.B. Janaki, *European Journal of Medicinal Chemistry* 49 (2012) 151-163.
- [13] K. Kumar, D. Awasthi, S.-Y. Lee, I. Zanardi, B. Ruzsicska, S. Knudson, P.J. Tonge, R.A. Slayden, I. Ojima, *Journal of Medicinal Chemistry* 54 (2011) 374-381.
- [14] C. Gill, G. Jadhav, M. Shaikh, R. Kale, A. Ghawalkar, D. Nagargoje, M. Shiradkar, *Bioorganic & Medicinal Chemistry Letters* 18 (2008) 6244-6247.
- [15] J. Camacho, A. Barazarte, N. Gamboa, J. Rodrigues, R. Rojas, A. Vaisberg, R. Gilman, J. Charris, *Bioorganic & Medicinal Chemistry* 19 (2011) 2023-2029.
- [16] D.G. Kokare, K. Naik, A. Nevrekar, A. Kotian, V. Kamat, V.K. Revankar, *Applied Organometallic Chemistry* (2016) n/a-n/a.
- [17] D.G. Kokare, V. Kamat, K. Naik, A. Nevrekar, A. Kotian, V.K. Revankar, *Journal of Molecular Structure*.
- [18] A. Jamadar, A.-K. Duhme-Klair, K. Vemuri, M. Sritharan, P. Dandawate, S. Padhye, *Dalton Transactions* 41 (2012) 9192-9201.
- [19] G.J. Kharadi, *Spectrochimica Acta Part A: Molecular and Biomolecular Spectroscopy* 79 (2011) 898-903.
- [20] S.P. Bruker, Bruker AXS Inc., Madison, Wisconsin, USA.
- [21] G. Sheldrick, *Acta Crystallographica Section A* 64 (2008) 112-122.
- [22] A. Spek, *Acta Crystallographica Section A* 46 (1990) c34.
- [23] C.F. Macrae, I.J. Bruno, J.A. Chisholm, P.R. Edgington, P. McCabe, E. Pidcock, L. Rodriguez-Monge, R. Taylor, J. van de Streek, P.A. Wood, *Journal of Applied Crystallography* 41 (2008) 466-470.
- [24] R.K. Verma, R. Mall, P. Ghosh, V. Kumar, *Synthetic Communications* 43 (2013) 1882-1895.
- [25] V. Kamat, K. Naik, V.K. Revankar, *Journal of Molecular Structure*.
- [26] M.V.N.d. Maria C. S. Lourenco, Alessandra C Pinheiro, Marcelle de L. Ferreira, Rasnisb B, Goncalves, Thais Cristina M Nogueira, Monica A Peralta., *ARKIVOC* 15 (2007) 181-191.
- [27] L. Collins, S.G. Franzblau, *Antimicrobial Agents and Chemotherapy* 41 (1997) 1004-1009.

- [28] M.a.G. Schwalve, CRC Press (2007).
- [29] M. Clark, R.D. Cramer, N. Van Opdenbosch, *Journal of Computational Chemistry* 10 (1989) 982-1012.
- [30] V. Thamilarasan, A. Jayamani, N. Sengottuvelan, *European Journal of Medicinal Chemistry* 89 (2015) 266-278.
- [31] A.N. Jain, *Journal of Computer-Aided Molecular Design* 10 427-440.
- [32] A.N. Jain, *Journal of Medicinal Chemistry* 46 (2003) 499-511.
- [33] X. He, A. Alian, R. Stroud, P.R. Ortiz de Montellano, *J Med Chem* 49 (2006) 6308-6323.
- [34] H.H. Freedman, *Journal of the American Chemical Society* 83 (1961) 2900-2905.
- [35] A. Kamath, S.P. Netalkar, D. Gangaram Kokare, K. Naik, V.K. Revankar, *Journal of Luminescence* 132 (2012) 2763-2768.
- [36] S.A. Galal, K.H. Hegab, A.S. Kassab, M.L. Rodriguez, S.M. Kerwin, A.-M.m.A. El-Khamry, H.I. El Diwani, *European Journal of Medicinal Chemistry* 44 (2009) 1500-1508.
- [37] S. Chandra, L.K. Gupta, *Spectrochimica Acta Part A: Molecular and Biomolecular Spectroscopy* 60 (2004) 3079-3085.
- [38] K. Nakamoto, *Infrared and Raman Spectra of Inorganic and Coordination Compounds: Part A: Theory and Applications in Inorganic Chemistry, Sixth Edition*, 2008.
- [39] I.H. Hall, N.J. Peaty, J.R. Henry, J. Easmon, G. Heinisch, G. Pürstinger, *Archiv der Pharmazie* 332 (1999) 115-123.
- [40] P.P. Netalkar, S.P. Netalkar, V.K. Revankar, *Applied Organometallic Chemistry* 29 (2015) 280-289.
- [41] A.B.P. Lever, *Inorganic Electronic Spectroscopy (2nd ed.)*, Elsevier, Amsterdam, Amsterdam, 1984.
- [42] W.A. Alves, S.A.d. Almeida-Filho, R.H.d.A. Santos, A. Paduan-Filho, A.M.d.C. Ferreira, *Journal of the Brazilian Chemical Society* 15 (2004) 872-883.
- [43] A.W. Addison, T.N. Rao, J. Reedijk, J. van Rijn, G.C. Verschoor, *Journal of the Chemical Society, Dalton Transactions* (1984) 1349-1356.
- [44] H. Okawa, M. Tadokoro, Y. Aratake, M. Ohba, K. Shindo, M. Mitsumi, M. Koikawa, M. Tomono, D.E. Fenton, *Journal of the Chemical Society, Dalton Transactions* (1993) 253-258.
- [45] B. Gold, H. Deng, R. Bryk, D. Vargas, D. Eliezer, J. Roberts, X. Jiang, C. Nathan, *Nat Chem Biol* 4 (2008) 609-616.
- [46] A.E. Hoffman, M. DeStefano, C. Shoen, K. Gopinath, D.F. Warner, M. Cynamon, R.P. Doyle, *European Journal of Medicinal Chemistry* 70 (2013) 589-593.
- [47] R.R. Zaky, K.M. Ibrahim, H.M. Abou El-Nadar, S.M. Abo-Zeid, *Spectrochimica Acta Part A: Molecular and Biomolecular Spectroscopy* 150 (2015) 40-53.
- [48] L. Ronconi, P.J. Sadler, *Coordination Chemistry Reviews* 251 (2007) 1633-1648.
- [49] K. Das, S. Nandi, S. Mondal, T. Askun, Z. Canturk, P. Celikboyun, C. Massera, E. Garribba, A. Datta, C. Sinha, T. Akitsu, *New Journal of Chemistry* 39 (2015) 1101-1114.
- [50] I.D. Kuntz, J.M. Blaney, S.J. Oatley, R. Langridge, T.E. Ferrin, *Journal of Molecular Biology* 161 (1982) 269-288.
- [51] I. Muegge, Y.C. Martin, *Journal of Medicinal Chemistry* 42 (1999) 791-804.
- [52] G. Jones, P. Willett, R.C. Glen, A.R. Leach, R. Taylor, *Journal of Molecular Biology* 267 (1997) 727-748.
- [53] M.D. Eldridge, C.W. Murray, T.R. Auton, G.V. Paolini, R.P. Mee, *Journal of Computer-Aided Molecular Design* 11 425-445.



Structures of Co(II), Cu(II) and Zn(II) complexes of 2-(2-(1H-benzo[d]imidazol-2-yl)hydrazono)propan-1-ol